Journal of Ovonic Research Vol. 19, No. 3, May - June 2023, p. 307 - 319

Enhanced resistance to degradation in sprayed perovskite $CH_3NH_3PbI_3$ induced by the temperature

A. Kamarchou[a] , A. Zobeidi[a.b], I. Kemerchou[c,d*], A.Khechekhouche[e] , A. Kaddour[f], B. Hammadi[g]
[a]*Pollution and waste treatment laboratory (PWTL), Kasdi Merbah Ouargla University .P.O. Box 511, Ouargla 30000, Algeria*
[b]*Department of Chemistry, Faculty of Exact Sciences, University of El-Oued, P.O. Box 789, El-Oued 39000, Algeria*
[c] *Applied mechanic and energy systems laboratoty (LMASE), Faculty of Applied Science, University of Ouargla, Ouargla 30000, Algeria*
[d]*Laboratory of Analysis and Control of Energy Systems and Networks, University of Laghouat, Laghouat, Algeria*
[e]*Technology Faculty, University of El Oued, El Oued 39000, Algeria.*
[f]*Laboratory of Biology, Environment and Health, Department of Biology, Faculty of Life and Natural Sciences, University of ElOued, Algeria*
[g]*Laboratory for the Valorization and Promotion of Saharan Resources, Faculty of Sciences, Technology and Material Sciences Kasdi Merbah Ouargla University, Algeria*

When compared to solar cells made from other materials, perovskites provided better performance in organic or inorganic hybrid solar cells. But one of the biggest problems facing scientists working in the photovoltaic industry right now is improving the stability of Perovskite solar cells. Despite their enormous potential, which exceeds that of traditional photovoltaic solar cells, these cells' low stability inhibits their commercialisation. In the current study, we looked at how the temperature of the substrate affected the physical characteristics of Perovskite thin films produced by spray pyrolysis using a moving nozzle. X-ray diffraction, scanning electron microscopy pictures, ultraviolet and visible absorption spectroscopy, and other methods were used to characterize the produced films. The results demonstrate that 90°C is the ideal deposition temperature.

(Received March 9, 2023; Accepted June 5, 2023)

Keywords: Perovskite thin films, Performance degradation, Stability, Spectrophotometer

1. Introduction

Worldwide, there has been an increasing need for renewable energy sources over the past decade, with solar energy being one of the most promising [1,2]. The focus of all researchers is the conversion of solar energy into electricity utilizing various materials-based solar cells and various solar cell designs. In the photovoltaic area, perovskite-based solar cells have recently attracted a lot of attention. Due to its optoelectronic characteristics, such as a high absorption coefficient, a long carrier-diffusion length, and the transportation of both electrons and holes, the perovskite material based on methylammonium lead triiodide ($CH_3NH_3PbI_3$) in particular emerges as a viable contender [3]. Consequently, $CH_3NH_3PbI_3$ is employed in a variety of gadgets, including photodiodes and light-emitting diodes [4, 5]. This material processing is often divided into physical and chemical processes, and it involves a number of steps, including the deposition of PbI_2 on coated glass, the conversion of PbI_2 to $CH_3NH_3PbI_3$, and the direct production of

* Corresponding author: kemerchou.imad@univ-ouargla.dz
https://doi.org/10.15251/JOR.2023.193.307

$CH_3NH_3PbI_3$ by sputtering [6–13]. The research of films characteristics [14], polarity and layer thickness [15], the impact of temperature [16, 17], and film deterioration [18–20] are the subject of a number of publications. According to recent reports, covering Perovskite film with a poly (methyl methacrylate) layer will protect it from oxygen and moisture. [21, 22]. As a result, thermal volatility is a very fascinating subject that continues to catch the interest of scientists working in the area. According to recent studies, the Perovskite layers that are produced on a substrate deteriorate over time at 95 °C in complete darkness. However, the findings demonstrate that the deterioration occurs at a temperature of 85 ° C in the inert environment. While the Perovskite films may thermally develop into PbI_2, CH_3NH_2, and HI gases when annealing temperatures are over 120 °C [21, 22]. The deterioration of Perovskite films is also significantly influenced by temperature and deposition technique. This study examines and discusses the impact of deposition temperature on the physical characteristics of thin films made of $CH_3NH_3PbI_3$. It is important to highlight that in order to demonstrate how temperature affects each film, we selected four samples of $CH_3NH_3PbI_3$ thin films made on glass substrates. The obtained findings demonstrate that samples kept in paper bags under dim lighting and processed earlier than three months retain their structural characteristics.

2. Experimental section

2.1. Preparation of PbI_2

500 ml of double-distilled water is combined with 35g of $PbICl_2$ and 70g of KI to create PbI_2. In accordance with the following Eq, the combination produces yellow PbI_2 (1):

$$PbCl2 + 2KI \rightarrow PbI2 + 2KCl \quad (1)$$

As will be demonstrated in section 3, XRD characterisation has been carried out to confirm the formation of PbI_2, and the spectrum is consistent with JCPDS No : 01.073-2234 (Space Group R-3c No. 167)

2.2. Preparation of CH_3NH_3I

30 ml of hydroiodic acid (HI: 57% wt water) and 27.8 ml of methylamine (MET: 40% wt in methanol) are combined in a beaker. The beaker is then put in an ice bath to keep its temperature at 0°C in order to prevent any complex reactions. In order to create a homogenous solution, the composite is also stirred for two hours. The resulting mixture of methanol and water is evaporated using a rotary evaporator for an hour at a temperature of 60°C. A yellow powder orange is eventually produced. This is then gathered and cleaned with diethyl ether until it is crystal clear white in color.

2.3. Preparation of $CH_3NH_3PbI_3$ layer

Figure 1 illustrates the stages involved in processing the $CH_3NH_3PbI_3$ material. The first step involves combining PbI_2 and CH_3NH_3I in 99% N.N. Dimethylformamide (DMF). Then, to create a homogenous solution, we stir the resulting solution for two hours at 60°C. Using spray pyrolysis with a moving nozzle, this will thereafter be deposited on various films heated at various temperatures (70°C, 80°C, 90°C, and 100°C) (SPMN). The resulting layers are heated for two hours at 100°C. [23-25].

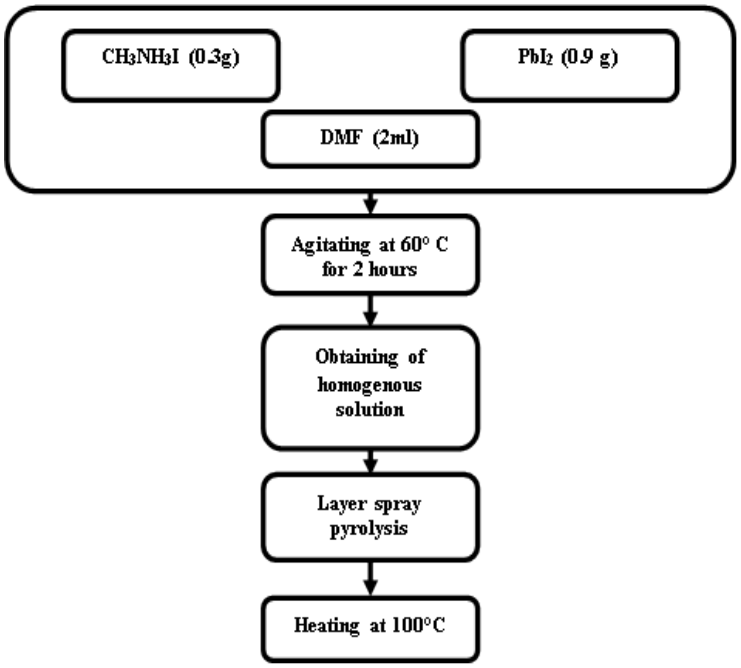

Fig. 1. Processing the $CH_3NH_3PbI_3$ material.

2.4 Thin film characterizations

A Philips X'pert pro-2 X-ray diffractometer equipment is used to study the crystalline structure of the generated $CH_3NH_3PbI_3$ thin films at various temperatures under various working circumstances, including 30 kV, 30 mA, and Cu K radiation with a wavelength of 1.5406 nm. Then, using Xpert High Score, the grain size may be calculated. As a result, the band gap energy is determined by employing the optical transmittance spectrum using a UV-visible spectrophotometer Shimadzu Model 1800 that operates between 300 and 900 nm in wavelength. The prepared samples' surfaces were examined using a scanning electron microscope (SEM) equipped with an FEI Quanta 250 and a tungsten filament. The $CH_3NH_3PbI_3$ thin film sample measurements and storage are carried out at room temperature. The samples are placed in paper pockets during storage to protect them from light. We repeat the measurements three months later to determine how the samples have degraded.

3. Results and discussions

The lead iodide powder's X-ray diffraction (XRD) spectrum is shown in Figure 2. (PbI_2) from 20° to

70°. According to JCPDS card No. 01.073-2234, a number of peaks are seen at 2, including 22.52°, 25.91°, 34.27°, 39.52°, and 45.18°, which, respectively, correspond to the diffraction planes (100), (101), (102), (110), and (103), of the PbI_2 phase. These outcomes demonstrate the prepared product's crystalline structure and demonstrate its suitability for use in producing our $CH_3NH_3PbI_3$ layers.

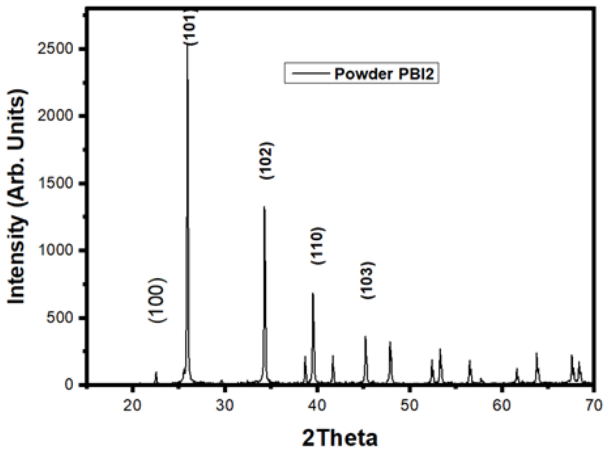

Fig. 2. X-ray results of Lead iodide powder.

Figure 3 displays the X-ray diffraction (XRD) patterns of $CH_3NH_3PbI_3$ films generated and aged at various temperatures. We have seen both of the sharpest peaks, which correspond to the (110) and (220) planes of perovskite, occur in freshly formed films at 2, 14.42°, and 28.74°. According to literary examples, these peaks signify the creation of the tetragonal Perovskite structure. [7]. While additional peaks ascribed to the diffraction planes (112), (202), (310), (021), (224), and (316) are present in the XRD patterns of various $CH_3NH_3PbI_3$ after age (330). From all spectral ranges, the two PbI2 peaks ((001) and (004)) lose strength. Therefore, the extra PbI_2 that may react with leftover CH_3NH_3 causes the (001) intensity to totally vanish from the films created at 70°C and 80°C. As a result, the observed spectrum proves that the SPMN-deposited material is entirely polycrystalline and supports the Perovskite structure. The remaining PbI_2 peaks, which are exhibited at 12.6° and 52.4° and correspond to the (001) and (004) planes, are also seen in the case of films with deposition temperatures of 70, 80, 90, and 100°C. The strongest peaks manifested at (110) and (220) planes in the case of sprayed Perovskite film entirely polycrystalline and supports the Perovskite structure. The remaining PbI_2 peaks, which are exhibited at 12.6° and 52.4° and correspond to the (001) and (004) planes, are also seen in the case of films with deposition temperatures of 70, 80, 90, and 100°C. The strongest peaks manifested at (110) and (220) planes in the case of sprayed Perovskite film prepared at 90°C are very sharp, indicating its high crystallinity. Also, peaks of PbI_2 become weak at deposition temperature of 90°C and heating value of 100°C conditions, which may be considered as adequate way to form high-$CH_3NH_3PbI_3$ stability.

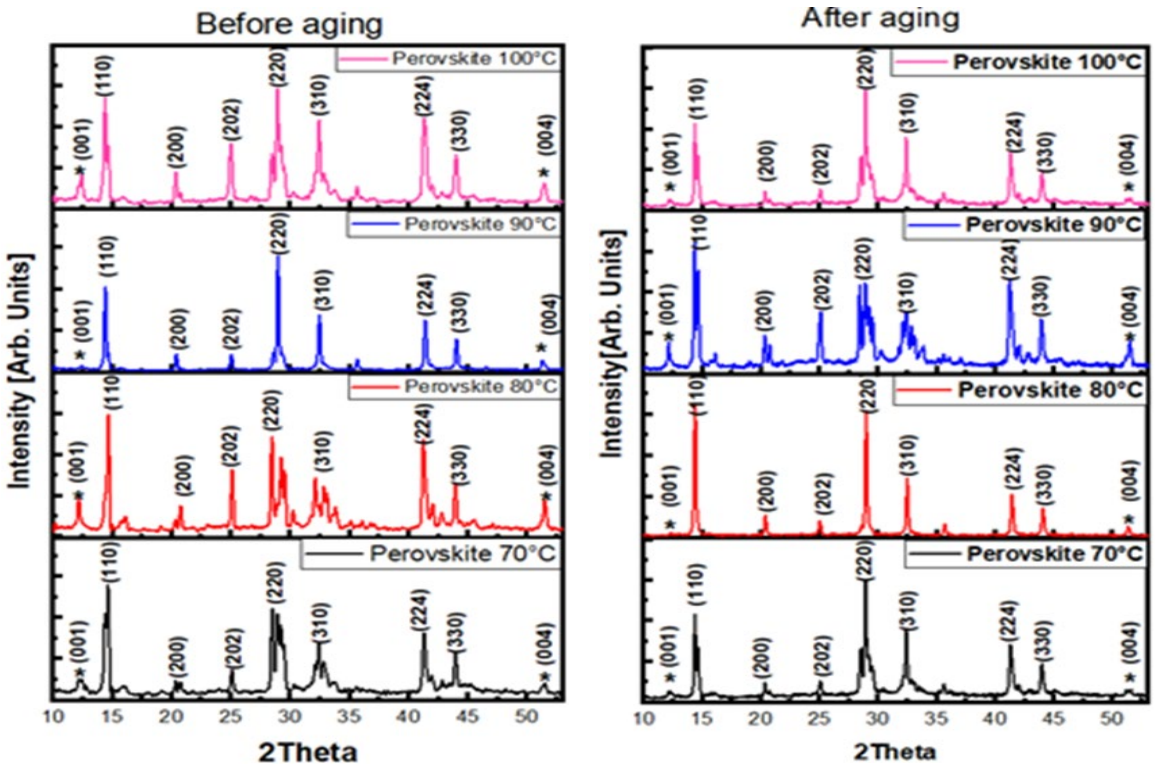

Fig. 3. X-ray results of $CH_3NH_3PbI_3$. a) before aging, b) after agin

Table 1 summarizes various parameters including d_{hkl}, 2θ, lattice parameters, and grain size of different deposition temperatures of Perovskite films. The inter-reticular distance d_{hkl}, lattice parameters (a and c), crystallites size D, stress μ, For the tetragonal Perovskite, the inter-reticular distance dhkl and the lattice constants a and c, are determined by the following expressions [26].

$$2d_{hkl}\sin(\theta) = n\lambda \tag{2}$$

Miller indices (hkl) of the Perovskite product before and after aging were determine from the five most intense peaks (110), (220), (310), (224), and (330).

$$\frac{1}{{d_{hkl}}^2} = \frac{1}{a^2}(h^2 + k^2) + \frac{l^2}{c^2} \tag{3}$$

$$\beta\cos\theta = \frac{k\lambda}{D} + \mu\sin\theta \tag{4}$$

k is assumed to be 0.9, whereas a and c are the lattice parameters. where = 1.054 is the wavelength of cooper K, is the full width at half medium in (rd), and is the diffraction angle in (°). The planes' Miller indices are h and kl, and the interplanar distance is d_{hkl}. With the help of Scherer's equation [5], which is provided by Eq. (5):

$$D = \frac{k\lambda}{\beta\cos\theta} \tag{5}$$

Table 1. hkl, 2θ, dhkl, lattice parameters, and grain size of the deposited $CH_3NH_3PbI_3$ layers before and after aging.

Deposition temperatures for 2 hours	*hkl*	*2θ* (°)	Calcul ted *d*[Å]	Lattice parameters a=b[Å]		Lattice parameters c[Å]		Unit cell volume V[Å^3] (A*b*c)/4		Grain size [nm]	
	110	14.360	6.16833	Before	After	Before	After	Before	After	Before	After
	220	28.449	3.13746	8.723	8.715	12.39	12.35	235.69		33.06	37.06
70 °C	310	32.418	2.76177						234.5		
	224	41.303	2.18591								
	330	43.984	2.05869								
	110	14.387	6.15669	8.706	8.71	12.37	12.35		234.23	37.30	43.15
	220	28.959	3.08337								
80 °C	310	32.456	2.75863					234.43			
	224	41.386	2.18173								
	330	44.017	2.05722								
	110	14.643	6.04961	8.555	8.73	12.704	12.65		241.02	41.48	42.52
	220	28.453	3.13705					232.46			
90 °C	310	32.102	2.78828								
	224	41.219	2.19020								
	330	43.920	2.06151								
	110	14.614	6.06138	8.572	8.72	12.63	12.42		236.09	41.20	56.52
	220	28.482	3.13374					232.01			
100 °C	310	32.400	2.76329								
	224	41.279	2.18714								
	330	43.942	2.05887								

Crystallite size changes D before and after aging are plotted in for further inquiry into the impact of preparation temperatures on various films. The figure shows that, prior to age, the crystallite size rises with deposition temperature and stays constant at 90°C and 100°C. This growth in crystallite size improves the film's crystallinity. In compared to before aging, the crystallite size grows larger after age. This can be explained by a decrease in PbI2 peaks in the aged Perovskite spectra. On the other hand, there is a chance that the excess PbI2 will react with any remaining CH3NH3 surplus to generate a layer of CH3NH3PbI3. The fluctuation of "cos" as a function of "sin" for various Perovskite layer deposition temperatures both before and after aging is shown in Figure 4. The slope of equation may be used to determine the extraction of different strains (4). As a result, Table 2 displays the values they acquired.

It is evident that not only the mode but also the difference applying potentials influenced the preferential orientation and also the cristallinity of the deposits [28].

The dislocation density of perovskite decreases after three months of storage in darkness for all produced samples (as shown in Table 2), resulting in larger grains.

Table 2. Micro strain values and density of Perovskite for different deposition temperatures before and after aging.

Various deposition temperatures for 2 hours	μ=Micro-strain before and after aging	Density of Perovskite CH3NH3PbI3 before and after aging1014 m-2
70 °C	0.00867/0.01562	9.13/9.13
80 °C	0.00238/0.00254	7.17/5.37
90 °C	-0.00315/0.0051	5.81/5.52
100°C	0.00682/0.00634	9.88/3.14

For this reason, the prepared layers are considered as an effective element for future solar cell applications.

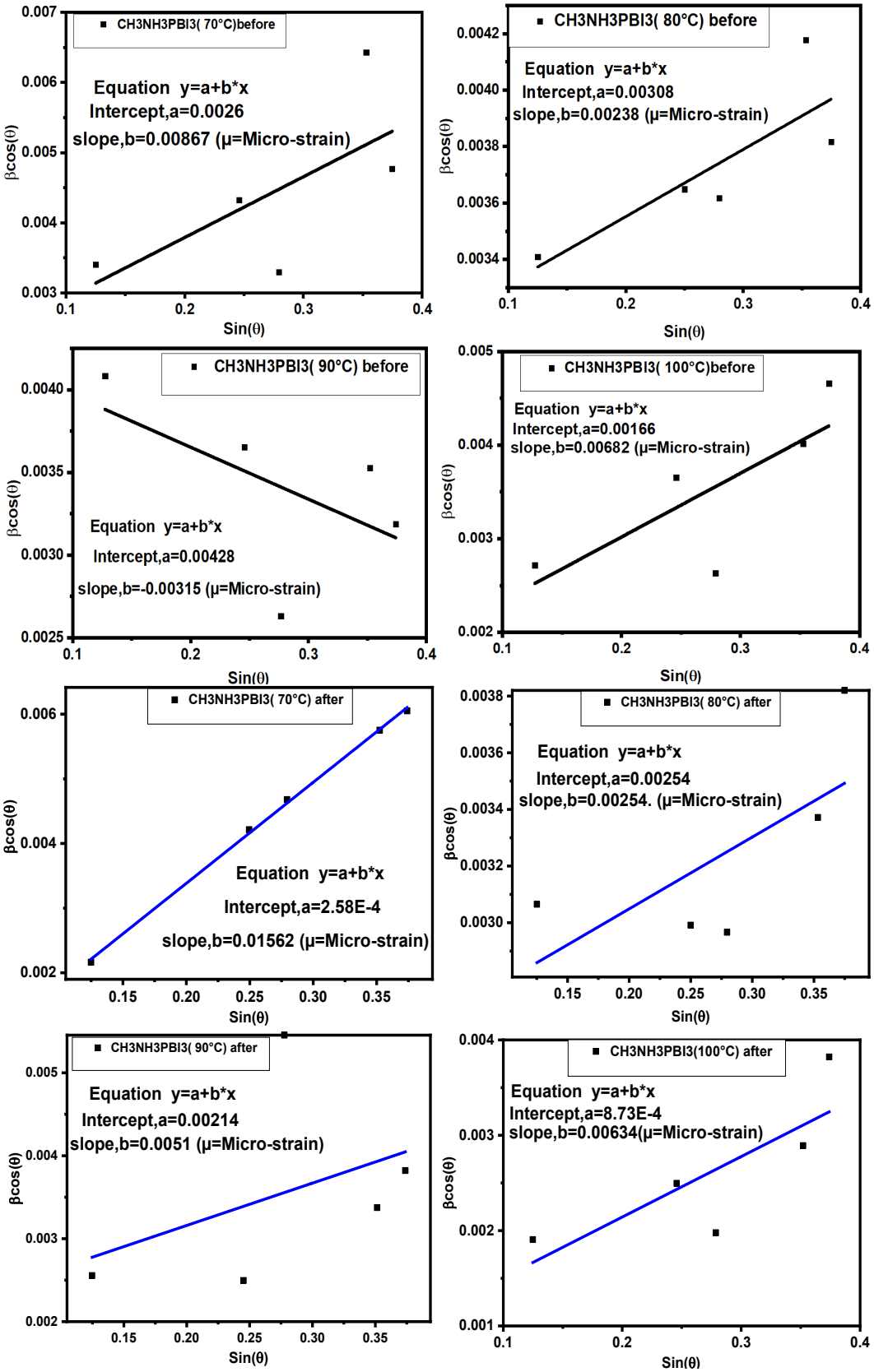

Fig. 4. Extraction of strain for different deposition temperatures of CH3NH3PbI3, layers before and after aging.

Figure 5 displays SEM images of Perovskite films that were sprayed at various processing temperatures. The Perovskite film made at 70°C, in contrast, had many pinholes and fissures that might result in substantial current leakage and charge recombination during the manufacturing of future solar cells.

SEM images of Perovskite distinguished spherical morphology and confirms the formation of particulate and porous films. The as deposited film was quite homogenous, it indicates clearly the particles to be roughly spherical and it shows areas richer in crystallites [27].

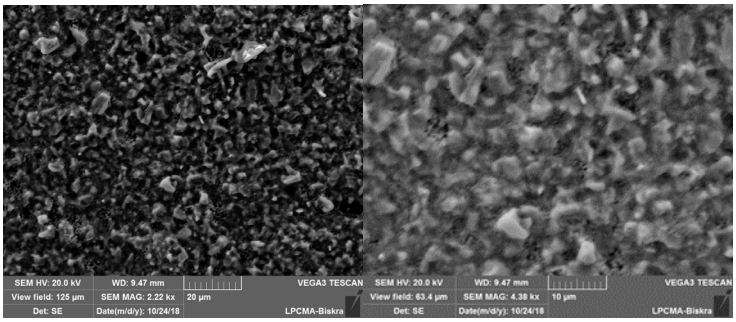

a. case of 70 °C

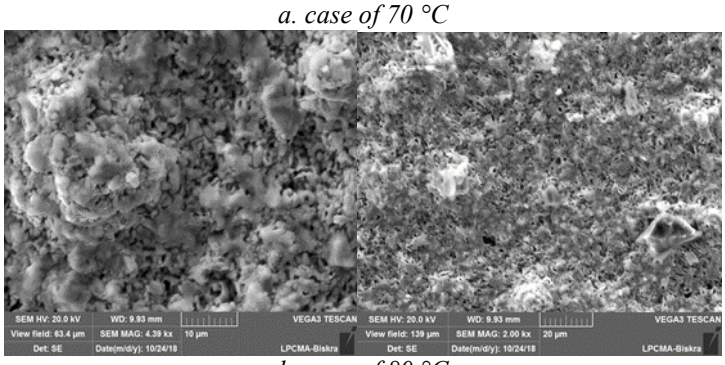

b. case of 80 °C

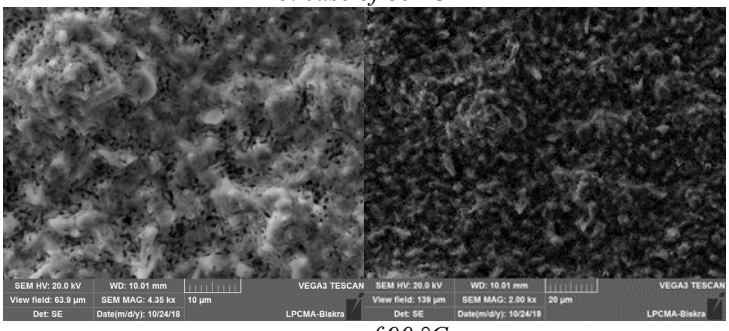

c. case of 90 °C

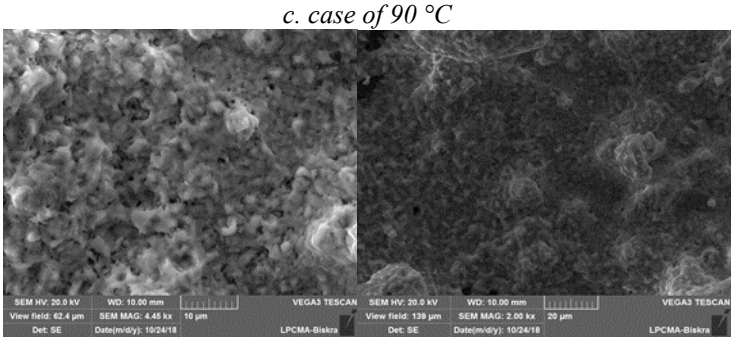

d. case of 100 °C

Fig. 5. SEM image under different processing temperature.

While all agglomerations are eliminated at a deposition temperature of 100°C. It is obvious that more uniform and plate-like structure is created at high processing temperatures, making interactions with other p-type molecules easier.

Figure 6 displays the CH3NH3PbI3 thin film absorbance fluctuation vs wavelength for various processing temperatures both before and after aging. For all conceivable preparation temperatures, the Perovskite thin films exhibit a high absorption range from 600 nm to 750 nm. According to absorption spectrometry, it is observed that the layer deposited at high temperatures (100 °C) has an optical absorbance greater than those deposited at temperatures 70 °C, 80 °C, and 90 °C, indicating the high crystallinity of the film. As the substrate time storage increases until 3 months after aging, the typical absorption becomes more spacious due to the Perovskite formation. As a result of the extraction of PbI2 from CH3NH3PbI3, films, the absorption range is expanded in comparison to that before aging. The produced Perovskite films may be employed as active layers for solar cell applications, which is a highly valuable result.

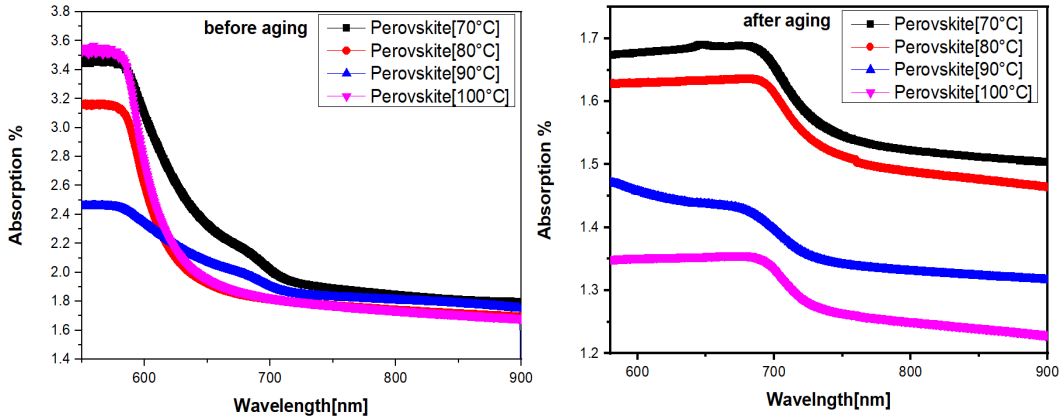

Fig. 6. Absorbance curve of Perovskite layers deposited at different temperatures before and after aging.

The band gap E_g values are deduced from transmission measurements using Tauc's relation given by Eq. (6):

$$(\alpha h\upsilon)^2 = B(h\upsilon - E_g) \tag{6}$$

The energy of a photon is h, where B is a constant. The fluctuation of (h)2 as a function of the photon energy (h) of perovskite for various processing temperatures is depicted in Figure .7. Extrapolating from the linear portion of the curve at (h)2=0 allows one to establish the optical band gap Eg of various layers. Figure 8 shows the band gap values at various processing temperatures as a result. The figure of 1.7 to 1.82 eV agrees well with the results that have been presented in the literature. The XRD's detection of PbI_2 phase is caused by the optical spectrum's absorption edges.

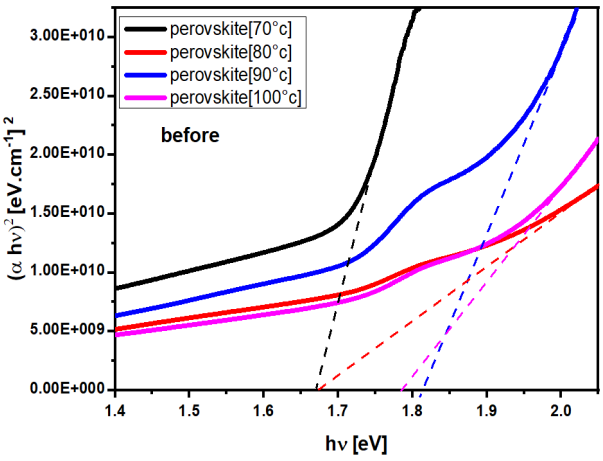

Fig. 7. Variation of $(\alpha h\upsilon)^2$ versus photon energy of Perovskite layers for different preparation temperatures before aging.

The Urback energy E_u is the main optical characteristic of thin-film layers, and it is calculated using the following Eq. (7):

$$\ln(\alpha) = \ln(\alpha_0) + \frac{h\nu}{E_u} \tag{7}$$

The variance against Perovskite for various processing temperatures is shown in Figure 8. Using the point where the abscise line and the straight line connect, we can calculate the reverse Urback energy from this curve.

Figure 9 also provides a summary of the Urback energy measurements made for various Perovskite layer processing temperatures. As processing temperature rises, the Urback energy value drops. This indicates that a crystalline structure with fewer imperfections is produced at the increased processing temperature.

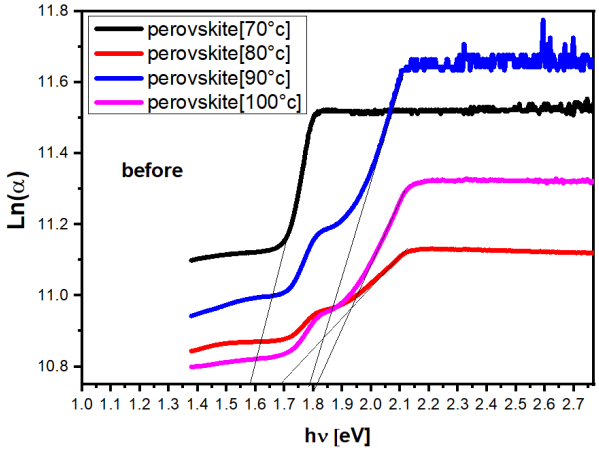

Fig. 8. Urback energy with various processing temperatures before aging.

Figure 9 shows how the urback and band gap energies vary with processing temperatures both before and after the cells are kept in the dark. It is obvious that the band gap energy is inversely related to the urback energy before the cells are held in the dark. As a result, as processing temperature rises from 70°C to 90°C, the band gap energy increases from 1.66 eV to 1.81 eV, respectively. However, with the same change in processing temperature indicated above,

the uraback energy falls from 0.63 eV to 0.55 eV. This is because the rate of absorption has increased and the amount of contaminants in manufactured cells has decreased. Additionally, at a processing temperature of 100 °C, a minor increase in Urback energy and a slight decrease in band gap energy value.

After three months of storage in the dark, it is shown that band gap energies drop at processing temperatures of 90 °C, 80 °C, and 100 °C, with a notable increase at 70 °C. However, regardless of the processing temperature, Urback energies values rise. The rise in crystal sizes is what causes the band gap energy to grow. On the other hand, an interaction between the organic and inorganic components results in the formation of the perovskite substance. Additionally, the prepared slides may be thought of as an active component in the production of stable cells. The best temperature for attaining good coverage and high crystallinity is 90°C, according to these results, which are in agreement with the XRD and UV studies.

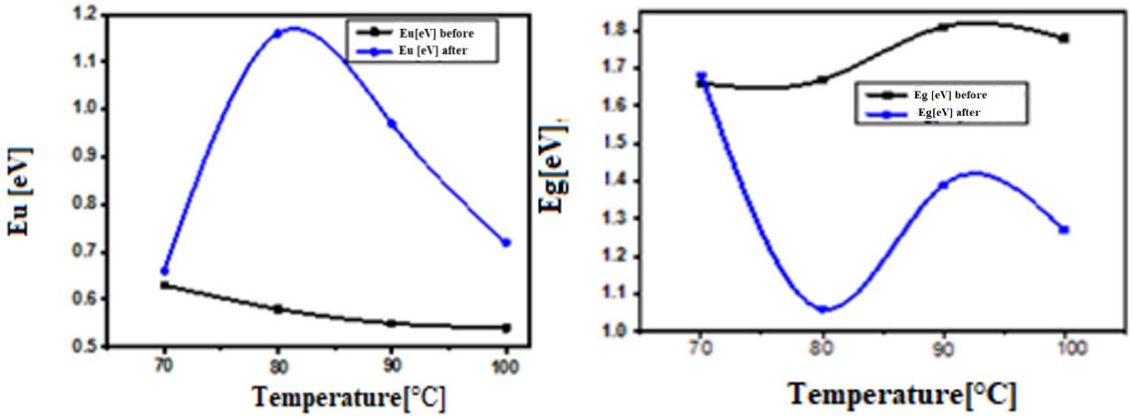

Fig. 9. Band gap and urback energies against various processing temperatures before and after aging.

4. Conclusion

XRD was used to show the structural characteristics of thin films made of $CH_3NH_3PbI_3$. The two most significant crystal peaks, peaks (110) and (220) show that the produced structure is made of tetragonal Perovskite. As a result, the temperature of 90 °C is the ideal deposition temperature that may be used to minimize the amount of surplus PbI_2. Additionally, when the crystals are deposited at higher temperatures, their size grows until it reaches a saturation point between 90 and 100 °C. This could improve the crystallinity of films. Additionally, due to the extraction of PbI_2 from $CH_3NH_3PbI_3$, films, the absorption range of various generated Perovskite layers is expanded in contrast to that before aging. Obtainable Perovskite films might serve as active layers in the future.

Acknowledgments

The VTRS Laboratory, the University of Technology, University of partly supported this work. Measurement of UV-visible data The X-ray diffraction data in this work were obtained using an XPERT-PRO diffractometer and is Supported by the University of Laghouat. PURF 2020 University of eloued .

References

[1] E. Kabir, P. Kumar, S. Kumar, A. A. Adelodun, and K.-H. Kim, Renewable and Sustainable Energy Reviews.82.894-900, (2018); https://doi.org/10.1016/j.rser.2017.09.094

[2] J. Gong, C. Li, and M. R. Wasielewski, Chemical Society Reviews.48.1862-1864, (2019). https://doi.org/10.1039/C9CS90020A

[3] T. Baikie, Y. Fang, J. M. Kadro, M. Schreyer, F. Wei, S. G. Mhaisalkar, et al., Journal of Materials Chemistry A.1.5628-5641, (2013); https://doi.org/10.1039/c3ta10518k

[4] M. Spina, L. Mihaly, K. Holczer, B. Nafradi, A. Pisoni, L. Forro, et al., ACS Appl Mater Interfaces.9.10198-10202, (Mar 22) (2017); https://doi.org/10.1021/acsami.6b12392

[5] S. Altazin, R. Clerc, R. Gwoziecki, G. Pananakakis, G. Ghibaudo, and C. Serbutoviez, Applied Physics Letters.99.143301, (2011); https://doi.org/10.1063/1.3643126

[6] G. Murugadoss, R. Thangamuthu, and S. M. S. Kumar, Solar Energy Materials and Solar Cells.164.56-62, (2017); https://doi.org/10.1016/j.solmat.2017.02.011

[7] Z. Yao, W. Wang, H. Shen, Y. Zhang, Q. Luo, X. Yin, et al., Science and Technology of advanced MaTerialS.18.253-262, (2017); https://doi.org/10.1080/14686996.2017.1298974

[8] J.-H. Im, H.-S. Kim, and N.-G. Park, APL Materials.2.081510, (2014); https://doi.org/10.1063/1.4891275

[9] N. Yantara, D. Sabba, F. Yanan, J. M. Kadro, T. Moehl, P. P. Boix, et al., Chemical Communications.51.4603-4606, (2015); https://doi.org/10.1039/C4CC09556A

[10] Z. Wang, S. Yuan, D. Li, F. Jin, R. Zhang, Y. Zhan, et al., Optics express.24.A1431-A1443, (2016); https://doi.org/10.1364/OE.24.0A1431

[11] C. Zhang, W. Luan, and Y. Yin, Energy Procedia.105.793-798, (2017); https://doi.org/10.1016/j.egypro.2017.03.391

[12] L. Zhou, J. Chang, Z. Liu, X. Sun, Z. Lin, D. Chen, et al., Nanoscale.10.3053-3059, (2018); https://doi.org/10.1039/C7NR07753J

[13] X. Du, Y. Wang, Z. G. Xia, and H. Zhou, Applied Mechanics and Materials, 2015, pp. 39-43; https://doi.org/10.4028/www.scientific.net/AMM.748.39

[14] I. Kemerchou, F. Rogti, B. Benhaoua, A. Hima, and A. Khechekhouche, Recueil de mécanique.4.342-348, (2019).

[15] A. Hima, A. Khechekhouche, I. Kemerchou, N. Lakhdar, B. Benhaoua, F. Rogti (2013).

[16] I. Kemerchou, F. Rogti, B. Benhaoua, N. Lakhdar, A. Hima, O. Benhaoua, et al., Journal Of Nano- and Electronic Physics 11.03011 (4), (2019); https://doi.org/10.21272/jnep.11(3).03011

[17] M. Taguchi, A. Suzuki, T. Oku, N. Ueoka, S. Minami, and M. Okita, Chemical Physics Letters.737.136822, (2019); https://doi.org/10.1016/j.cplett.2019.136822

[18] L. Xu, R. Molaei Imenabadi, W. G. Vandenberghe, and J. W. P. Hsu, APL Materials.6.036104, (2018); https://doi.org/10.1063/1.5021138

[19] A. Alberti, I. Deretzis, G. Mannino, E. Smecca, S. Sanzaro, Y. Numata, et al., The Journal of Physical Chemistry C.121.13577-13585, (2017); https://doi.org/10.1021/acs.jpcc.7b04196

[20] S. Wang, Y. Jiang, Emilio J. Juarez-Perez, Luis K. Ono, and Y. Qi, Nature Energy.2.16195, (2016); https://doi.org/10.1038/nenergy.2016.195

[21] D. Shan, G. Tong, Y. Cao, M. Tang, J. Xu, L. Yu, et al., Nanoscale Research Letters.14.208, (2019); https://doi.org/10.1186/s11671-019-3022-y

[22] M. Taguchi, A. Suzuki, H. Tanaka, and T. Oku, "Fabrication and characterization of perovskite solar cells added with MnCl2, YCl3 or poly (methyl methacrylate)," in AIP Conference Proceedings, 2018, p. 020012; https://doi.org/10.1063/1.5021925

[23] W. Zhao, Z. Yao, F. Yu, D. Yang, and S. F. Liu, Adv Sci (Weinh).5.1700131, (Feb) (2018); https://doi.org/10.1002/advs.201700131

[24] M.-R. Ahmadian-Yazdi, A. Rahimzadeh, Z. Chouqi, Y. Miao, and M. Eslamian, AIP Advances.8.025109, (2018); https://doi.org/10.1063/1.5019784

[25] S. Heo, G. Seo, Y. Lee, D. Lee, M. Seol, J. Lee, et al., Energy & Environmental

Science.10.1128-1133, (2017); https://doi.org/10.1039/C7EE00303J

[26] L. Dghoughi, B. Elidrissi, C. Bernede, M. Addou, M. A. Lamrani, M. Regragui, et al., Applied Surface Science.253.1823-1829, (2006); https://doi.org/10.1016/j.apsusc.2006.03.021

[27] F. Rahala,b, A. Kamarchouc, A. Berchia, D. Abdia, I. Kemerchoud, Journal of Ovonic Research. P , 661-668, (2022), https://doi.org/10.15251/JOR.2022.185.661

[28] A. Kamarchou, S. Atia, A. Zobeidi, H. Chettah, S. Benhamidad, D. Abdic, F. Rahalc, A. Berchic, N. Chaabiac Chalcogenide Letters, July 2022, p. 447 - 456, https://doi.org/10.15251/CL.2022.197.447